Journal of Applied Mechanics and Technical Physics, Vol. 36, No. 5, 1995

NUMERICAL SOLUTION OF NAVIER–STOKES EQUATIONS FOR AN INCOMPRESSIBLE LIQUID IN CHANNELS WITH A POROUS INSERT

N. T. Danaev, Sh. Smagulov, and N. M. Temirbekov

UDC 519.6:532.516

This work is devoted to a numerical investigation of stationary flows in curvilinear channels with a porous insert. An iterative algorithm is considered, for which it is established that the number of iterations, if the calculation process is convergent, depends weakly on the hydraulic permeability value of the porous layer. Data of the numerical computations and their analysis are given.

In mathematical simulation of the laminar flow of an isothermal incompressible liquid in channels with a porous insert, which is a partition packed by beads of equal diameter, the following system of equations is widely used [1–4]:

$$\rho\Big(\frac{\partial U^i}{\partial t}+\sum_{k=1}^{3} U^k\frac{\partial U^i}{\partial x^k}\Big)+\frac{\partial P}{\partial x^i}=\sum_{k=1}^{3}\frac{\partial}{\partial x^k}\Big[\mu_{\text{ef}}\Big(\frac{\partial U^i}{\partial x^k}+\frac{\partial U^k}{\partial x^i}\Big)\Big]-\frac{\mu U^i}{R},\quad i=1,2,3,\qquad \operatorname{div}\mathbf{u}=0,$$

where $\mathbf{u}=(U^1,U^2,U^3)$ is the velocity vector, P is the pressure, ρ is the density, and μ is the coefficient of dynamic viscosity. In this case the term $\mu\mathbf{u}/R$ takes into account the friction forces arising in the porous region due to the presence of a solid phase (beads). To relate the viscous stress tensor to the velocity vector components the notion of effective viscosity μ_{ef} is introduced in the same way as is done in discribing turbulent flows.

In verification of the model described above the determination of the value of μ_{ef}, which is widely different in the literature, presents the greatest difficulty. For example, in [1] it is proposed to choose μ_{ef} in the form

$$\mu_{\text{ef}}=\mu\Big[1+2.5\Big(\frac{1}{\varepsilon}-1\Big)+A\frac{(1-\varepsilon)^2}{\varepsilon^3}\Big],$$

where A is an empirical coefficient, whose numerical value should be adopted by comparing the calculated and experimental data ($A=30$–35), whereas in [2] μ_{ef} is taken in the from

$$\mu_{\text{ef}}=\begin{cases}\xi\mu(1\leqslant\xi\leqslant 200) & \text{inside the porous layer,}\\ \mu & \text{outside the layer.}\end{cases}$$

Thus the adoption of a reasonable coefficient μ_{ef} is in itself an independent problem of mathematical simulation. In addition, a comparison of calculation results for a direct-flow reactor with a fixed granulated layer, reported in [1–4], with different values of μ_{ef} (in [3, 4] $\mu_{\text{ef}}=\mu=\text{const}$) shows that they coincide qualitatively. Comparison of quantitative characteristics with physical data is hindered, since no experiments have been published in which the continuous development of the flow in channels with a porous insert is studied in detail. Furthermore, although attempts have been undertaken to measure characteristics inside the granulated layer, these data frequently disagree, which is primarily due to difficulties in measurements inside the layer [5–7].

Kazakh State National University, Almaty 480046. Translated from Prikladnaya Mekhanika i Tekhnicheskaya Fizika, Vol. 36, No. 5, pp. 21–29, September–October, 1995. Original article submitted September 28, 1994.

 0021-8944/95/3605-0658 $12.50

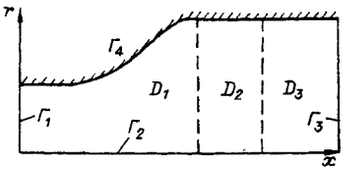

Fig. 1

In this connection, to get the most reliable picture of liquid flow through porous media it is worthwhile to conduct investigations on the basis of simple mathematical models that allow an effective computational realization. In the present work, flows of an incompressible liquid with a constant viscosity coefficient through porous inserts in axisymmetric channels with curvilinear boundaries are studied on the basis of the stationary Navier–Stokes equations.

To describe the stationary flows of viscous incompressible liquid in curvilinear boundary channels with a porous insert, the Navier–Stokes equations in the variables (Ψ, Ω) can be written in cylindrical coordinates as

$$\frac{\partial U\Omega}{\partial x} - \frac{\partial V\Omega}{\partial r} = \frac{1}{\mathrm{Re}}\left(\Delta\Omega + \frac{\partial}{\partial r}\left(\frac{\Omega}{r}\right)\right) - \mathrm{div}\left(\frac{k}{r}\,\mathrm{grad}\,\Psi\right), \qquad \mathrm{div}\left(\frac{1}{r}\,\mathrm{grad}\,\Psi\right) = \Omega, \tag{1}$$

where

$$U = \frac{\partial\Psi}{\partial x}; \quad V = -\frac{1}{r}\frac{\partial\Psi}{\partial r}; \quad \Omega = \frac{\partial U}{\partial r} - \frac{\partial V}{\partial x}; \qquad k(x,r) = \begin{cases} 0 & \text{in } D_1 \cup D_3, \\ k_0(x,r) & \text{in } D_2; \end{cases}$$

and $k_0(x,r)$ is the hydraulic permeability of the porous medium.

We consider the following boundary conditions for the curvilinear domain $D = D_1 \cup D_2 \cup D_3$, shown in Fig. 1:

at the inlet boundary Γ_1

$$\Psi = \Psi_0(r), \quad \Omega = \Omega_0(r) \quad (\Psi_0, \Omega_0 \text{ are known functions});$$

at the symmetry axis Γ_2

$$\Psi = \Omega = 0;$$

at the outlet boundary Γ_3, located "far" enough from the porous insert, we assume that $\partial\Psi/\partial x = \partial\Omega/\partial x = 0$, i.e., impose "soft" boundary conditions;

at the solid wall Γ_4

$$\Psi = \mathrm{const}, \quad \frac{\partial\Psi}{\partial n} = 0. \tag{2}$$

In the orthogonal curvilinear coordinate system, system (1) can be written as

$$(L_1 + L_2)\,\Omega = -L_3\Psi; \tag{3}$$

$$\frac{\partial}{\partial q^1}\left(\frac{\Phi}{r}\frac{\partial\Psi}{\partial q^1}\right) + \frac{\partial}{\partial q^2}\left(\frac{1}{r\,\Phi}\frac{\partial\Psi}{\partial q^2}\right) = J\Omega. \tag{4}$$

Here

$$L_1\Omega = \frac{\partial}{\partial q^1}\left[\frac{1}{r}\left(\frac{\partial\Psi}{\partial q^2} + \frac{a_{12}}{\mathrm{Re}}\right)\Omega\right] - \frac{1}{\mathrm{Re}}\left(\frac{\partial}{\partial q^1}\,\Phi\frac{\partial\Omega}{\partial q^1}\right);$$

$$L_2\Omega = \frac{\partial}{\partial q^2}\left[\frac{1}{r}\left(\frac{\partial\Psi}{\partial q^1} + \frac{a_{11}}{\mathrm{Re}}\right)\Omega\right] - \frac{1}{\mathrm{Re}}\left(\frac{\partial}{\partial q^2}\,\Phi^{-1}\frac{\partial\Omega}{\partial q^2}\right);$$

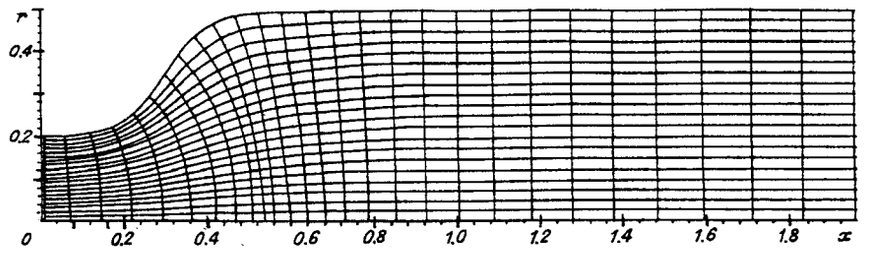

Fig. 2

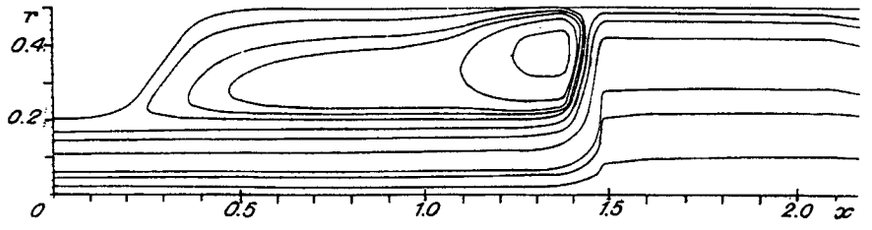

Fig. 3

$$L_3\Psi = \frac{\partial}{\partial q^1}\left(k\frac{\Phi}{r}\frac{\partial\Psi}{\partial q^1}\right) + \frac{\partial}{\partial q^2}\left(k\frac{1}{r\Phi}\frac{\partial\Psi}{\partial q^2}\right);$$

$$\Phi = \sqrt{g_{22}/g_{11}}\,; \quad a_{ij} = \frac{\partial x^i}{\partial q^j} \quad (i,j=1,2); \quad J = \sqrt{g_{11}\,g_{22}}\,.$$

The hydraulic permeability of the porous medium was taken into account by the expression

$$k_0 = \frac{150\,(1-\varepsilon)^2}{\mathrm{Re}\,\varepsilon^3}\,G^2\,, \quad G = d_a/d\,,$$

where ε is the porosity coefficient, d_a is the inner channel diameter, and d is the characteristic diameter of granules of the porous material.

For numerical construction of a curvilinear grid in the calculational domain, the method described in [8] was used.

In Fig. 2, a finite-difference curvilinear grid is depicted for a domain that is characteristic for the boundary problems under consideration. While verifying the orthogonality of this grid it was found that

$$\max|\,g_{12}/\sqrt{g_{11}g_{22}}\,| \leqslant 0.0288\,.$$

To solve numerically the system of differential equations (3) and (4), we consider the following finite-difference iteration splitting scheme [9]:

$$\frac{\Omega^{n+1/3}-\Omega^n}{\tau} + L_{1,h}\,\Omega^{n+1/3} + L_{2,h}\,\Omega^n = -(L_{3,h}-A_h)\Psi^n\,, \tag{5}$$

$$\frac{\Omega^{n+2/3}-\Omega^n}{\tau} + L_{1,h}\,\Omega^{n+1/3} + L_{2,h}\,\Omega^{n+2/3} = -(L_{3,h}-A_h)\Psi^n\,, \tag{6}$$

$$\frac{\Omega^{n+1}-\Omega^{n+2/3}}{\tau} = -(L_{3,h}-A_h)(\Psi^{n+1}-\Psi^n)\,, \tag{7}$$

$$\left(\frac{\Phi}{r}\,\Psi^{n+1}_{q^1}\right)_{\bar{q}^1} + \left(\frac{1}{\Phi r}\,\Psi^{n+1}_{q^2}\right)_{\bar{q}^2} = J\Omega^{n+1}\,. \tag{8}$$

Here $L_{1,h}$, $L_{2,h}$, and $L_{3,h}$ are difference equivalents of the differential operators L_1, L_2, and L_3, in which

convective terms are approximated with due regard to the sign of the flow velocity; the operator A_h has a structure determined by the procedure of introducting an auxiliary function, described in [10].

The boundary condition (2) at a solid wall is taken into account by the Toma formula

$$\Omega_{k,N_2} = \frac{1}{h_2^2} \frac{-2(\Psi_{\bar{q}^2})_{k,N_2-1/2}}{r_{k,N_2-1/2}(g_{22})_{k,N_2-1/2}}, \tag{9}$$

where $(g_{22})_{k,N_2-1/2} = (x^1_{\bar{q}^2,k,N_2-1/2})^2 + (x^2_{\bar{q}^2,k,N_2-1/2})^2$.

The algorithm of the suggested method is as follows:

1. In the first stage, from relations (5) and (6), which have uniform boundary conditions, we find the values of $\Omega^{n+2/3}$ inside the computational domain by the scalar sweep method,

2. Then, using expression (8), we exclude Ω^{n+1} from relation (7) and obtain a finite-difference equation for determining Ψ^{n+1}:

$$\frac{1}{J}\left\{ \left(\frac{\Phi}{r} \Psi^{n+1}_{q^1} \right)_{\bar{q}^1} + \left(\frac{1}{\Phi r} \Psi^{n+1}_{q^2} \right)_{\bar{q}^2} \right\} - \tau(L_{3,h} - A_h)\Psi^{n+1} = \Omega^{n+2/3} + \tau(L_{3,h} - A_h)\Psi^n, \tag{10}$$

which is solved at the given boundary conditions by the iteration overrelaxation method;

3. After finding Ψ^{n+1} inside the grid domain D, we determine Ω^{n+1} from formula (8).

In doing so, the calculations by the finite difference scheme (5)–(8) at the given initial approximation Ψ^0 are continued until a steady-state criterion is fulfilled:

$$\max |\Omega^{n+1} - \Omega^n| \leqslant \tau\varepsilon, \quad \mathbf{x} \in D_h, \tag{11}$$

where ε is a preset quantity characterizing the accuracy of iteration. If the steady-state criterion is fulfilled, the final values of vorticity on the boundary are calculated from formula (9).

At the channel inlet, the values of the stream function and of vorticity are given by the expressions

$$\Psi = -\frac{r^4}{2a^2} + r, \quad \Omega = -\frac{4}{a^2} r.$$

The computations by the scheme (5)–(10) were initially performed for the grid shown in Fig. 2 at $\tau = 0.05$; the grid points were 41×21. The numerical calculations were carried out for the following values of porosity coefficient:

1) $\varepsilon(r) = 1$ at $0 \leqslant r \leqslant 0.5$;

2) $$\varepsilon(r) = \begin{cases} 0.5 & \text{at } 0 \leqslant r \leqslant 0.2, \\ (100r^2 + 101)/210 & \text{at } 0.2 \leqslant r \leqslant 0.5; \end{cases}$$

3) $$\varepsilon(r) = \begin{cases} 0.4 & \text{at } 0 \leqslant r \leqslant 0.2, \\ (10r^2 - 4r + 4)/9 & \text{at } 0.2 \leqslant r \leqslant 0.5; \end{cases}$$

4) $$\varepsilon(r) = \begin{cases} 0.38 & \text{at } 0 \leqslant r \leqslant 0.2, \\ (0.62r^2 - 0.124r + 0.38) & \text{at } 0.2 \leqslant r \leqslant 0.5; \end{cases}$$

5) $$\varepsilon(r) = \begin{cases} 0.3 & \text{at } 0 \leqslant r \leqslant 0.2, \\ (100r^2 + 59)/210 & \text{at } 0.2 \leqslant r \leqslant 0.5; \end{cases}$$

6) $$\varepsilon(r) = \begin{cases} 0.2 & \text{at } 0 \leqslant r \leqslant 0.2, \\ (50r^2 - 20r + 11)/45 & \text{at } 0.2 \leqslant r \leqslant 0.5. \end{cases}$$

Some results of the calculations for different variants of choice of $\varepsilon(r)$ for Re = 100 are given in Table 1. Here $k_{\max}$ is the maximal value of the drag coefficient of the porous medium, $\varepsilon_{\min}$ and $\varepsilon_{\max}$ are the minimal and maximal porosity values of the layer, and N is the number of iterations. All the computations were performed on a BESM-6 computer in the same initial approximation until inequality (11) with $\varepsilon = 10^{-3}$ was

TABLE 1

Variant No.	k_{max}	ε_{min}	ε_{max}	N
1	0	1.0	1.0	97
2	300.0	0.5	0.5	110
3	843.7	0.4	0.5	112
4	1050.8	0.38	0.473	113
5	2722.0	0.3	0.4	117
6	12000.0	0.2	0.3	145

TABLE 2

Re	x_{max}	y_{max}	Ψ_{max}
100	0.0599	0.3540	0.02204
500	1.3761	0.3748	0.02931
1000	1.4062	0.3998	0.03801

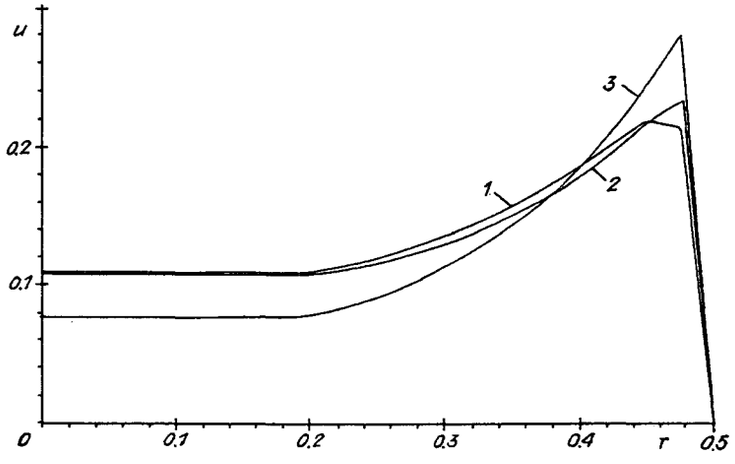

Fig. 4

fulfilled. As is seen from Table 1, the number of iterations necessary to fulfill the steady-state criterion (11) depends only slightly on the permeability variations of the porous layer.

A set of isolines of the stream function for Re = 1000 is given in Fig. 3. From Fig. 3 and also from the calculations for Re = 100, 500 it is seen that, as a viscose gas flows through porous media, a vortex zone appears in the expanding sections of the diffuser. This zone occupies a vast space close to the porous insert and its size increases with increasing Re.

Figure 4 shows radial profiles of the axial velocity component inside the porous layer at different values of the porosity coefficient: curves 1–3 are the profiles for the second, fifth, and sixth variants of ε, respectively. From the profiles it is seen that the nonuniformity of the velocity over the channel vertical cross section inside the porous insert increases with decrease in the porosity coefficient, i.e., with increase in the porous medium drag.

Table 2 gives the coordinates of the center of the recirculation zone and the values of Ψ at the center for different Re. It is seen that with increase in Re the center of the recirculation zone moves toward the top corner in front of the porous insert, and the value of Ψ_{max} increases, i.e., the vorticity becomes more intense.

In the following calculations we consider the case of a channel with a cuvilinear boundary given by the Vitoshinskii function, which is widely used in practice:

$$r = \frac{r_0}{\sqrt{1 - \left(1 - \left(\frac{r_0}{r_1}\right)^2\right) \frac{(1 - 3x^2/a^2)^2}{(1 + 3x^2/a^2)^3}}}, \qquad 0 \leqslant x \leqslant a/\sqrt{3}.$$

Here r_1 is the radius of the inlet section, r_0 is the radius of the outlet section, x is the coordinate along the

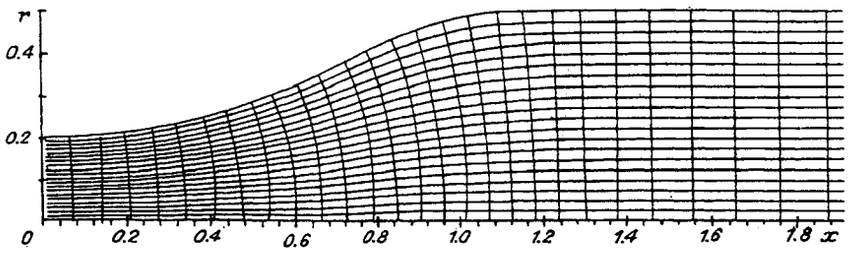

Fig. 5

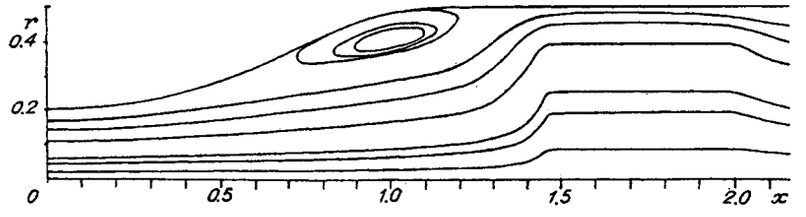

Fig. 6

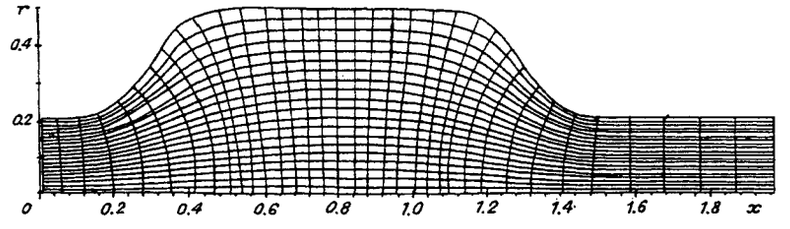

Fig. 7

channel axis; and the parameter a is usually taken to be $4r_0$. The case where $r_0 = 0.5$, $r_1 = 0.2$, and $x_l = 4.0$ is considered below.

The calculation results for domain (12) are given in Figs. 8 and 9. Isolines of the stream function and of the vorticity for Re = 250, $\varepsilon = 0.4$ are shown in Fig. 8a,b. The vorticity on the solid wall for different values of Re is given in Fig. 9, where lines 1–3 correspond to Re=1000, 500, and 100 at $\varepsilon = 0.2$–0.3. Note that with increase in Re the value of the vorticity on the wall ahead of the porous insert increases.

In Fig. 5, a computational domain for the Vitoshinskii channel is shown, and an orthogonal curvilinear grid is constructed. Figure 6 shows the flow pattern inside the Vitoshinskii channel with a porous insert for Re = 100 and $\varepsilon = 0.38$–0.43.

The results of the numerical calculations suggest that for small Reynolds numbers ($\mathrm{Re} \leqslant 60$) separation-free flow is established in the diffusers of the Vitoshinskii channel, whereas for $\mathrm{Re} \geqslant 100$ the recirculation zone appears in front of the porous insert.

Finally we consider the case of an expanding–contracting channel with a computational domain bounded by the lines

$$x = 0\,, \qquad x = 2.5, \qquad r = 0\,,$$

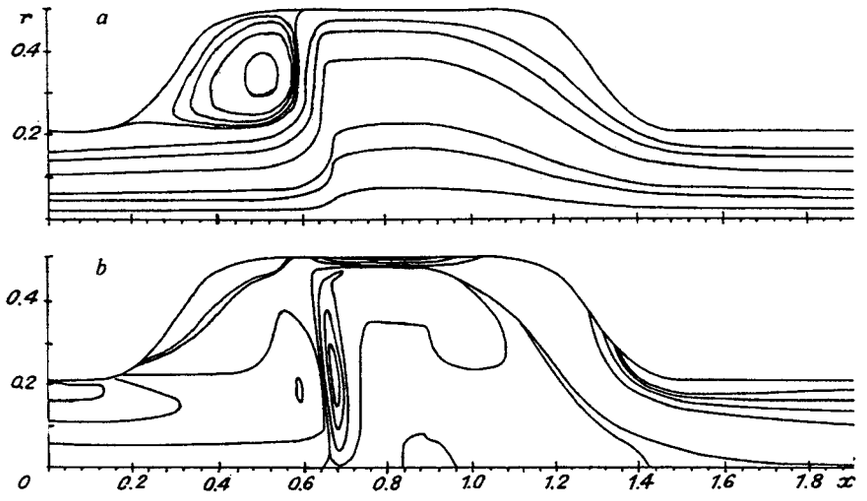

Fig. 8

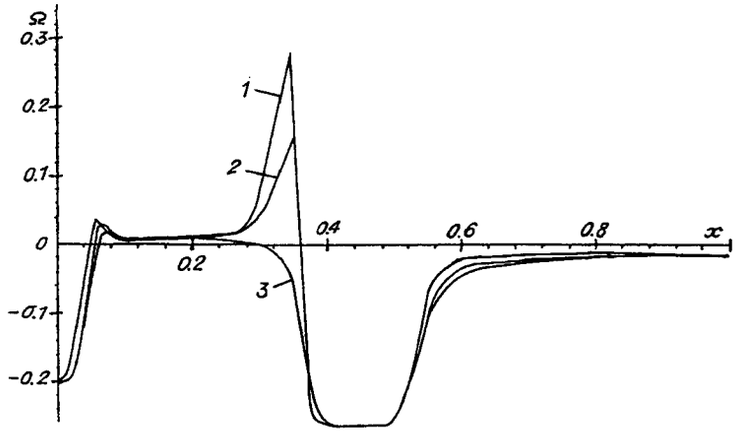

Fig. 9

$$r = \frac{a+b}{2} + \frac{a-b}{2}\tanh\left(R(x-x_0)\right) = f_1(x) \quad \text{at} \quad 0 \leqslant x \leqslant 0.6\,,$$
$$r = \frac{a+b}{2} + \frac{a-b}{2}\tanh\left(R(x_{0p}-x)\right) = f_2(x) \quad \text{at} \quad 1 \leqslant x \leqslant 1.5\,, \tag{12}$$
$$r = f_1(0,6) \quad \text{at} \quad 0.6 \leqslant x \leqslant 1, \qquad r = f_2(1.5) \quad \text{at} \quad 1.5 \leqslant x \leqslant 2.5 \qquad (x_0 = 0.3\,, \quad x_{0p} = 1.3)\,.$$

This domain and the curvilinear grid arrangement are shown in Fig. 7.

The calculation results for a domain given by relations (12) are shown in Figs. 8 and 9. The isolines of the stream function and the vorticity at Re = 250, $\varepsilon = 0.4$ are shown in Fig. 8a,b. The vorticity on the solid wall for different values of Re is given in Fig. 9, where lines 1–3 correspond to Re=1000, 500, and 100 at $\varepsilon = 0.2$–0.3. Note that with increase in Re the value of the vorticity at the wall ahead of the porous insert increases.

The numerous calculation results suggest that the flow inside channels with a porous insert is vortical, and the vortex is generated as a result of interaction of the flowing medium with the porous material. In near-wall flows, the generation and diffusion of vortices originate from the channel walls. Increase in the value

of the drag coefficient of the porous material with constant Reynolds numbers affect only slightly the volume of the vortex zone, because the porous insert is placed far from the diffuser part of the channel.

On the basis of the computations performed it was also established that:

— at any set of determining parameters a retardation of the liquid flow takes place in front of the porous insert;

— the character of the flow through the granulated layer over the horizontal cross sections of the insert is close to one-dimensional and depends weakly on the character of liquid supply (at a constant flow rate);

— the appearance of nonuniformities of the longitudinal velocity component is revealed in the form of so-called "ears," which strongly depend on the porosity coefficient.

REFERENCES

1. I. V. Shirko, "Numerical simulation of flows in granulated media," in: *Numerical Simulation in Aerodynamics* [in Russian], Nauka, Moskow (1986), pp. 236–245.
2. B. P. Gerasimov, P. S. Demeshev, A. A. Ionkin, and A. G. Churbanov, "Numerical investigation of hydrodynamics and heat exchange in porous media," Preprint No. 185, Inst. Appl. Math., Academy of Sciences of the USSR, Moscow (1987).
3. N. M. Temirbekov, "Numerical simulation of hydrodynamics of a viscous gas in a channel with a porous insert," in: *Theory of Functions, Equations of Mathematical Physics, and Applications*, Alma-Ata (1987), pp 54–58.
4. N. T. Danaev, Sh. A. Ershin, U. K. Zhapbaslaev, and M. Sh. Kulumbaeva, "Numerical investigation of motion of a viscous incompressible liquid in a channel with a porous barrier," *Vestn. Akad. Nauk Kaz. SSR*, No. 10, 64–70 (1987).
5. V. E. Nakoryakov, V. A. Mukhin, and V. I. Volkov, "Experimental investigation of velocity field in a stationary granulated layer," in: *Transition Processes in Apparatus of Chemical Energy Production* [in Russian], Novosibirsk (1985), pp. 138–150.
6. W. Jonston, A. Dyblos, and R. Edvards, "Measurement of fluid velosity inside porous media with laser anemometer," *Phys. Fluids.*, **18**, No. 7, 913–914 (1975).
7. M. E. Aerov, O. M. Todes, and D. A. Narinskii, *Apparatuses with a Stationary Granulated Layer* [in Russian], Khimiya, Leningrad (1975).
8. N. T. Danaev, "On the possibility of numerical construction of orthogonal grids," in: *Numerical Methods of Continuum Mechanics* [in Russian], Institute of Theoretical and Applied Mechanics, Sibirian Division, Academy of Sceince of the USSR, **14**, No. 3 (1983), pp. 42–53.
9. P. N. Vabishevich, "Realization of boundary conditions in solving the Navier–Stokes equations in 'stream function, and vorticity' variables," *Dokl. Akad. Nauk SSSR*, **273**, No. 1, 22–26 (1983).
10. N. T. Danaev and Sh. Smagulov, "About a method of the numerical solution of the Navier–Stokes equations in (ψ, φ) variables," in: *Simulation in Mechanics* [in Russian], Institute of Theoretical and Applied Mechanics, Sibirian Division, Academy of Sceince of the USSR, **5**, No. 4 (1991), pp. 38–47.